American Society of Mechanical Engineers

ASME Accepted Manuscript Repository

Institutional Repository Cover Sheet

Cranfield Collection of E-Research - CERES

ASME Paper Title: A characteristic-based 1D axial compressor model for stall and surge simulations

Authors: Kissoon S, Righi M, Pawsey L, Pachidis V, Tunstall R, Roumeliotis I

ASME Conf Title: ASME Turbo Expo 2023: Turbomachinery Technical Conference and Exposition

Volume/Issue: 13A Turbomachinery Date of Publication (VOR* Online): 28 September 2023

ASME Digital Collection URL: https://asmedigitalcollection.asme.org/GT/proceedings-abstract/GT2023/87080/V13AT29A002/1168506

DOI: 10.1115/GT2023-100709

*VOR (version of record)

Proceedings of ASME Turbo Expo 2023
Turbomachinery Technical Conference and Exposition
GT2023
June 26-30, 2023, Boston, Massachusetts
DOI: 10.1115/GT2023-100709

GT2023-100709

A CHARACTERISTIC-BASED 1D AXIAL COMPRESSOR MODEL FOR STALL AND SURGE SIMULATIONS

Sajal Kissoon
Cranfield University
Bedfordshire, UK

Mauro Righi
Cranfield University
Bedfordshire, UK

Lucas Pawsey
Rolls-Royce plc.
Bristol, UK

Vassilios Pachidis
Cranfield University
Bedfordshire, UK

Richard Tunstall
Rolls-Royce plc.
Bristol, UK

Ioannis Roumeliotis
Cranfield University
Bedfordshire, UK

ABSTRACT

A low-order unsteady one-dimensional axial compressor and combustor model has been developed at Cranfield University as part of a larger unsteady gas turbine engine model, with the ability to simulate compressor stall and surge. The flow is resolved using the 1D unsteady Euler equations and source terms are used to model bleed extraction (and addition), pressure losses, and heat and work exchange. Species tracking is used in the combustor part of the model, using a semi-coupled approach, to keep track of the combustion products and unburnt fuel in the main gas path. The equations are solved using a Roe Approximate Riemann Solver, modified to handle the high magnitude, transient source terms necessary for this simulation. The performance of the compressor during the transient surge event is described by a set of compressor characteristics, including reverse flow and rotating stall regions, obtained from a validated 3D throughflow code, ACRoSS. To replicate the exact response of multi-stage compressors, stage-by-stage characteristics are used during reverse flow.

The low-order method presented is successfully verified against ACRoSS for a high-power surge event of a coupled IPC and HPC configuration. The rate at which the total pressure at the outlet of the HPC collapses was calculated to be within 1%. This approach presents a faster alternative to high-fidelity CFD and can be used to investigate the compressor stall behaviour within minutes during the early design phase.

Keywords: stall, surge, one-dimension, numerical model, multi-stage, axial compressor, transient simulation.

NOMENCLATURE

~	Grid Interface
ρ	Density
γ	Ratio of specific heat
α	Wave strength
λ	Eigenvectors
ϵ	Internal energy
a	Speed of sound
A	Cross-sectional area
C_v	Specific heat at constant volume
e	Total energy per unit volume/eigenvalues
E	Internal energy
F	Flux Euler matrix/Momentum
H	Enthalpy
P	Total pressure
Q	Heat addition
R	Gas Constant
S	Source terms
SW	Shaft work
t	Time
T	Total temperature
u	Stream velocity
U	Conservative Euler matrix
W	Mass flow
y	Velocity fraction
Y	Mass fraction
NRT	Non-dimensional speed
PR	Pressure ratio
TR	Temperature Ratio
WRTP	Non-dimensional mass flow

Subscripts

B	Bleed
comb	Combustor
comp	Compressor
F	Fuel
i	Grid node
L	Left cell
R	Right cell

Published by The American Society of Mechanical Engineers. This is the Author Accepted Manuscript issued with:
Creative Commons Attribution License (CC BY). The final published version is available online at DOI: 10.1115/GT2023-100709.
Please refer to any applicable publisher terms of use.

1. INTRODUCTION

The occurrence of stall and surge represents the breakdown of orderly flow through a compressor which leads to a sudden drop in pressure rise. This highly dynamic and transient phenomenon leads to a loss of thrust in aero-engines and, if sustained, is often accompanied by major engine damage. It plagued the late 1940s and early 1950s due to the fast-paced advancements made in compressor design towards performance and efficiency at the expense of operability. The onset of surge and stall was at that time seen as "pulsating flows and other forms of unsteadiness." [1] This kickstarted 80 years of research into understanding and predicting the occurrence of stall. Although its commencement, development and consequence on the engine is still not fully understood, the exponential development of computational power opened the possibility of improving the understanding of this phenomena without being restricted by the limitations of instrumentations. Following recent developments in computational fluid dynamics and experimental methods, the nature of research into stall and surge is transitioning from being descriptive to predictive.

Post-stall behaviour can be subdivided into two types: rotating stall and surge. Rotating stall is distinguished by one or more cells of low axial velocity rotating circumferentially around the compressor, at lower speed than the rotor. Surge is instead the complete axi-symmetric flow reversal. A deep surge can be distinguished from a classical surge when the mass flow recorded temporarily becomes negative. In such conditions, the compressor faces severe mechanical and thermal loads which usually happen in a cyclic manner with high amplitudes. Through the collaborative effort of aerodynamicists, control specialists, structural and performance engineers, engine compressors are now less prone to surging. However, this was achieved at the expense of a higher stall margin which limits the operating range and design space of compressors. Also, it restricts research towards new compressor designs which might be more prone to sudden stalling problems. Engine manufacturers are hence generally constrained to start from successful compressor designs and adapt them for different engine configurations based on proprietary rules-of-thumb. This approach, albeit less risky, hinders step changes in gas turbine design. Hence, predicting compressor response, post-stall, at low computational cost, would open the design space and reduce testing costs as this allows for new compressor configurations to be tested right at the initial stages of design.

Early modelling work was based on lumped parameter models which represented components of the compression system [2-6]. However, these models have only been used on low-speed compressors. At higher speeds, the compressibility effects become more prominent which reduces accuracy. Three-dimensional through-flow models have been developed but were only validated against experimental data from low-speed compressors [7-11] due to the complexities associated with simulating surge events on experimental rigs [14]. Although 3D CFD models were set up to simulate stall in high-speed and transonic axial compressors [12,13,31] it was only recently that Righi et. al successfully validated ACRoSS for surge against a 5-stage high-speed rig which is representative of the front stages of a modern high-pressure compressor (HPC) [14]. This milestone allowed for the generation of compressor characteristics which can be used in a low-order model.

This paper proposes a novel, unsteady, one-dimensional axial compressor, and combustor model, for the simulation of one or more compressors, post-stall at various power settings. The components have been developed as part of a whole engine simulation transient tool for shaft failure and overspeed conducted within Cranfield University. It will help estimate transient engine response following the sudden decoupling of the compressor with its turbine and predict levels of overspeed for certification purposes. The low-order compressor model uses characteristics which includes: unstalled, stalled, and reverse flow regions. Those compressor maps are generated using a three-dimensional, through-flow code called ACRoSS, Axial Compressor Rotating Stall and Surge simulator [30]. To the best of the authors' knowledge, this is the first published case of a stand-alone, one-dimensional, axial compressor model capable of simulating high power surge events for multi-stage axial compressors.

2. METHODOLOGY

2.1 Roe Scheme

Stall and surge events consist of highly dynamic flow, recirculating or going in opposite directions. They often lead to steep gradients in flow properties across compressors. For this application, Roe's linearized approximate Riemann solver scheme [15] is adapted to solve the Euler equations. Also, being monotonicity preserving, Roe's scheme avoids spurious oscillation in locations where a discontinuity is present. Due to its popularity, the scheme has been refined throughout the years and applied to a wide range of physical problems [16]. The original Roe scheme was modified to include an entropy fix to resolve issues arising due to the computation of rarefaction shocks [17-20].

To replicate the flow inside an axial compressor and combustor, the Euler equations was modified to include source terms to represent:

- fuel mass addition (W_F) and bleed ($\pm W_B$)
- change in momentum due to secondary flow (F_B, F_F), work addition (F_{comp}) and pressure loss (F_{comb}, F_{loss})
- changes in cross-sectional area
- energy removal and addition from bleed (H_B), compressor (SW), fuel addition (H_F) and combustion (Q).

Figure 1 illustrates a typical control volume of a compressor and combustor.

The governing equations for this flow can be written in the following form:

$$(\boldsymbol{AU})_t + (\boldsymbol{AF})_x = \boldsymbol{S} \qquad (1)$$

Where

$$\boldsymbol{U} = \begin{Bmatrix} \rho \\ \rho u \\ e \end{Bmatrix} \quad (2)$$

$$\boldsymbol{F} = \begin{Bmatrix} \rho u \\ \rho u^2 + p \\ u(e+p) \end{Bmatrix} \quad (3)$$

Total internal energy, *e*, is defined using specific enthalpy, h, as a function of temperature and mass flow fractions to account for combustion products and unburnt fuel. This is later explained further.

$$e = E + \frac{u^2}{2} \quad (4)$$

$$E = h - RT \quad (5)$$

$$\text{h} = \text{f(T) and H} = \text{h} + \frac{u^2}{2} \quad (6)$$

The vector *S* is given by the following equation and considers changes in mass, momentum and energy associated with the different sources.

$$\boldsymbol{S} = \begin{Bmatrix} W_F - W_B \\ F_{comp} - F_{comb} - F_B + F_F - F_{loss} + p\frac{dA}{dx} \\ SW + Q - H_B + H_F \end{Bmatrix} \quad (7)$$

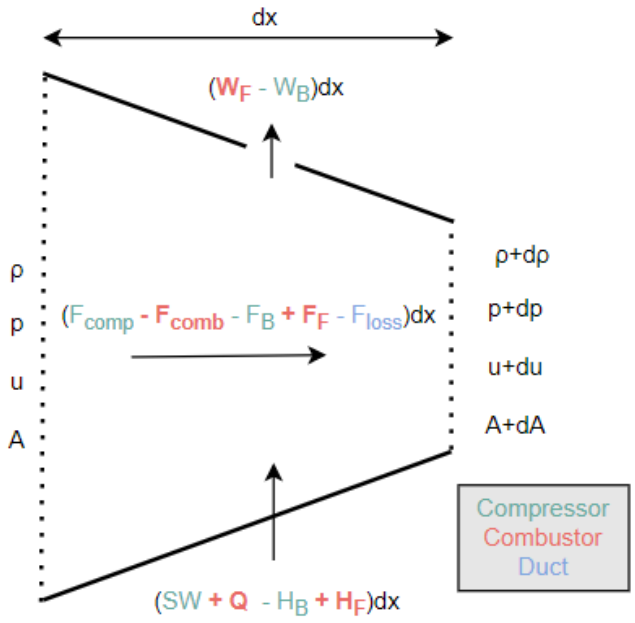


FIGURE 1: CONTROL VOLUME FOR A ONE-DIMENSIONAL FLOW FOR A COMPRESSOR AND COMBUSTOR

The governing equations assume that the changes in properties of the main gas path, due to the introduction or removal of fuel or bleed, become uniform instantaneously and that complete mixing is done at the elemental control volume itself. Also, the source terms assume that there are no derivatives of flow variables. During 1D combustion, heat is artificially added to the flow and reactivity of the species are not modelled. A pressure drop within the hot section of the combustor is defined as an input through F_{comb}.

The wave strengths within the Roe's Riemann solver need to be modified to prevent excessive oscillations of the results. This is discussed by Roe [34]. This is a particularly important modification due to the big magnitude of the source terms which are introduced within just a few nodes. The wave strengths are modified for a quasi-one-dimensional flow governed by equation 1. From the compatibility relations in the theory of characteristics, as outlined by Mohanraj et al., the differential changes in flow properties can be obtained [22]. This includes the strength of the entropy wave and the left and right acoustic waves. Hence, for a generalized quasi-one-dimensional flow, the compatibility relations are:

$$dp - a^2 d\rho = \psi dt \quad (8)$$

along the path line,

$$dp - \rho a du = \left[-\frac{\rho u a^2}{A}\frac{dA}{dx} + a^2\varepsilon - a\beta + \psi\right] dt \quad (9)$$

along the left running Mach wave and

$$dp + \rho a du = \left[-\frac{\rho u a^2}{A}\frac{dA}{dx} + a^2\varepsilon + a\beta + \psi\right] dt \quad (10)$$

along the right running Mach wave, where

$$\varepsilon = \frac{1}{A}\left[\frac{d\dot{W}_F}{dx} - \frac{d\dot{W}_B}{dx}\right] \quad (11)$$

$$\beta = \frac{1}{\tilde{A}}\left(F_{comp} - F_{comb} - F_{loss} - u(1-y_F)\frac{d\dot{m}_F}{dx} - u(1-y_B)\frac{d\dot{m}_B}{dx}\right) \quad (12)$$

$$\psi = (\gamma - 1)\left[\rho u\frac{\delta Q}{dx} - dH_F - dH_B - u\beta\right] \quad (13)$$

$$dH_{F/B} = \frac{[H - H_{F/B}]}{A}\frac{d\dot{m}_{F/B}}{dx} \quad (14)$$

$$\text{y} = \frac{u_{F/B}}{u} \quad (15)$$

Equations for the wave strength are thus derived by first multiplying equation 6 by $-1/\tilde{a}^2$ and equations 7 and 8 by $\frac{1}{2}\tilde{a}^2$ and then substituting in the compatibility equations 6-8. The wave strength, as defined by equations 14-16, can then be obtained by having its definition on the left-hand side and a homogeneous expression on the right.

$$\tilde{\alpha}_1 = \frac{1}{2\tilde{a}^2}(dp - \tilde{\rho}\tilde{a}du) \tag{16}$$

$$\tilde{\alpha}_2 = \frac{1}{\tilde{a}^2}(\tilde{a}^2 d\rho - dp) \tag{17}$$

$$\tilde{\alpha}_1 = \frac{1}{2\tilde{a}^2}(dp + \tilde{\rho}\tilde{a}du) \tag{18}$$

The equations for the wave strengths are modified and obtained from equations 16-18 as follows:

$$\tilde{\alpha}_1 = \frac{1}{2\tilde{a}^2}\Big[dp - \tilde{\rho}\tilde{a}du + \frac{1}{\tilde{u}-\tilde{a}}\Big(\tilde{\rho}\tilde{u}\tilde{a}^2\frac{dA}{\tilde{A}} - (\gamma-1)\tilde{\rho}\tilde{u}\delta Q + [(\gamma-1)\tilde{u}+\tilde{a}]\tilde{f}_x - \frac{w_f}{\tilde{A}}\Big(\tilde{u}(1-y_f)[(\gamma-1)\tilde{u}+\tilde{a}] + \tilde{a}^2 - (\gamma-1)(\tilde{H}-H_f)\Big) + \frac{w_b}{\tilde{A}}\Big(\tilde{u}(1-y_b)[(\gamma-1)\tilde{u}+\tilde{a}] + \tilde{a}^2 - (\gamma-1)(\tilde{H}-H_b)\Big)\Big)\Big] \tag{19}$$

$$\tilde{\alpha}_2 = \frac{1}{\tilde{a}^2}\Big[\tilde{a}^2 d\rho - dp + (\gamma-1)\Big[\tilde{\rho}\delta Q - \tilde{f}_x + \frac{w_f}{\tilde{u}\tilde{A}}\Big(\tilde{u}\big(1-y_f\big) - \big(\tilde{H}-H_f\big)\Big) - \frac{w_b}{\tilde{u}\tilde{A}}\Big(\tilde{u}(1-y_b) - \big(\tilde{H}-H_b\big)\Big)\Big]\Big] \tag{20}$$

$$\tilde{\alpha}_3 = \frac{1}{2\tilde{a}^2}\Big[dp + \tilde{\rho}\tilde{a}du + \frac{1}{\tilde{u}+\tilde{a}}\Big(\tilde{\rho}\tilde{u}\tilde{a}^2\frac{dA}{\tilde{A}} - (\gamma-1)\tilde{\rho}\tilde{u}\delta Q + [(\gamma-1)\tilde{u}-\tilde{a}]\tilde{f}_x - \frac{w_f}{\tilde{A}}\Big(\tilde{u}(1-y_f)[(\gamma-1)\tilde{u}-\tilde{a}] + \tilde{a}^2 - (\gamma-1)(\tilde{H}-H_f)\Big) + \frac{w_b}{\tilde{A}}\Big(\tilde{u}(1-y_b)[(\gamma-1)\tilde{u}-\tilde{a}] + \tilde{a}^2 - (\gamma-1)(\tilde{H}-H_b)\Big)\Big)\Big] \tag{21}$$

The interface flux can then be computed through equation 17 which averages, by considering the wave strength the resulting flux at the interface between elemental control volumes:

$$F_{i+\frac{1}{2}} = \frac{1}{2}\big(F_L + F_R - \textstyle\sum_k \alpha_k|\tilde{\lambda}_k|e_k\big) \tag{22}$$

The eigenvalues and eigenvectors of the Jacobian matrix which considers the pair of states U_L and U_R are:

$$e_1 = \big\{1,\ \tilde{u}-\tilde{a},\ \tilde{H}-\tilde{u}\tilde{a}\big\}^T \tag{23}$$

$$e_2 = \Big\{1,\ \tilde{u},\ \frac{\tilde{u}^2}{2}\Big\}^T \tag{24}$$

$$e_3 = \big\{1,\ \tilde{u}+\tilde{a},\ \tilde{H}+\tilde{u}\tilde{a}\big\}^T \tag{25}$$

$$\tilde{\lambda}_1 = \tilde{u}-\tilde{a} \tag{26}$$

$$\tilde{\lambda}_2 = \tilde{u} \tag{27}$$

$$\tilde{\lambda}_3 = \tilde{u}+\tilde{a} \tag{28}$$

Through an explicit, Euler forward scheme, the conserved variables U at the next time-step can be obtained by discretizing equation 1 as follows:

$$\frac{(AU)_i^{n+1}-(AU)_i^n}{\Delta t} + \frac{(AF)^n_{i+\frac{1}{2}}-(AF)^n_{i-\frac{1}{2}}}{\Delta x} = g_i(S) \tag{29}$$

where $g_i(S)$ can be obtained as follows for a first-order accurate scheme in space.

$$g_i(S) = \frac{1}{4}(S_{i-1} + 2S_i + S_{i+1}) \tag{30}$$

Although the modified simple Roe scheme presented is only first-order accurate, literature has shown [32,33] that it is sufficient for the purpose of this study and that further improvement in the order would not provide enough accuracy to justify the increase in computational cost.

To avoid the occurrence of transonic expansion shocks, the eigenvalues are modified according to the method proposed by Harten and Hyman [23], known as entropy fix, as follows:

$$\begin{cases} |\tilde{\lambda}_k| = |\tilde{\lambda}_k| & |\tilde{\lambda}_k| \geq \frac{\delta\tilde{\lambda}_k}{2} \\ |\tilde{\lambda}_k| = \frac{\tilde{\lambda}_k{}^2}{\tilde{\lambda}_k} + \frac{\tilde{\lambda}_k}{4} & |\tilde{\lambda}_k| < \frac{\delta\tilde{\lambda}_k}{2} \end{cases} \tag{31}$$

$$\begin{cases} \frac{\delta\tilde{\lambda}_k}{2} = 0, & k = 2 \\ \frac{\delta\tilde{\lambda}_k}{2} = \min\{\tilde{a}, \max[0,2(\lambda_{k,R} - \lambda_{k,L})]\}, & k = 1,3 \end{cases} \tag{32}$$

The Roe average gas properties were modified according to the methodology proposed by Di Mare [24] which considers the temperature and changes in static internal energy between the left and right control volumes as follows:

$$\begin{cases} \tilde{C}_v = C_v & T_L = T_R \\ \tilde{C}_v = \frac{\epsilon_R - \epsilon_L}{T_R - T_L} & T_L \neq T_R \end{cases} \tag{33}$$

$$\tilde{\gamma} = \frac{R+\tilde{C}_v}{\tilde{C}_v} \tag{34}$$

Due to fuel being introduced and burnt within the combustor, the combustion products lead to a change in gas properties. Species tracking was introduced within the compressor and combustor model to integrate this change in gas properties which will affect the performance of a whole engine model. Also, the slight change in density at the nozzle guide vane will affect the flow capacity which could lead to noticeable changes in surge frequency. The additional species considered are combustion products and unburnt fuel in addition to air.

However, the introduction of two new species requires extensive modification to the Jacobian matrix. Given that the species are non-reactive, the "Uncoupled Approach" outlined by Larrouturou [25] and used by [26] was integrated. This method offers a lower computational cost and reduced complexity compared to the fully coupled approach, at the cost of a lower accuracy. However, this is acceptable for this application as the total mass of the species are low compared to the main gas path. Additionally, it has the appeal of maintaining the mass fraction Y positive.

Considering that the species have the following relationship where Y = mass flow of component/total mass flow,

$$Y_{air} + Y_{unburnt\ fuel} + Y_{combustion\ products} = 1 \quad (35)$$

Larrouturou's uncoupled approach consists of treating the Euler equations and an additional species equation separately at each timestep.

$$(\rho Y)_t + (\rho u Y)_x = 0 \quad (36)$$

Using a frozen value of γ, the flux is calculated with

$$\gamma_{i+\frac{1}{2}} = \gamma\left(\frac{Y_i^n + Y_{i+1}^n}{2}\right) \quad (37)$$

$$u_{i+\frac{1}{2}}^n = \frac{1}{2}(u_i^n + u_{i+1}^n) \quad (38)$$

The flux component relating to the changes in composition is then obtained by:

$$F_{i+\frac{1}{2}}^4 = u_{i+\frac{1}{2}}^n \times \begin{cases} (\rho Y)_i^n & if\ u_{i+\frac{1}{2}}^n > 0, \\ (\rho Y)_i^n & if\ u_{i+\frac{1}{2}}^n < 0. \end{cases} \quad (39)$$

Once the U matrix is obtained from the Roe solver (equation 29), gas properties are extracted from it as shown below.

$$\rho = U_1 \quad (40)$$

$$u = \frac{U_2}{U_1} \quad (41)$$

$$e = \frac{U_3}{U_1} - \frac{U_2^2}{2U_1^2} \quad (42)$$

$$Y_{SP} = \frac{U_4}{U_1} \quad (43)$$

$$Y_{FNB} = \frac{U_5}{U_1} \quad (44)$$

The static temperature is solved iteratively by first guessing it from the specific internal energy, *e*. Then using the enthalpy routine which calculates specific enthalpy using the mass fraction of the combustion products the static temperature is obtained iteratively through the secant method over the error term.

$$t_{guess} = \frac{e}{C_p - R} \quad (45)$$

$$T = \frac{1-(h-Rt_{guess})}{e} \quad where\ h = f(t_{guess}) \quad (46)$$

The static pressure is then calculated from the static temperature using the ideal gas law.

A summary of the computational steps used to implement the Roe scheme is shown in Figure 2. The timestep is computed based on the Courant–Friedrichs–Lewy (CFL) condition and the source terms associated with the compressor and combustor are evaluated and explained in sections 2.2 and 2.4.

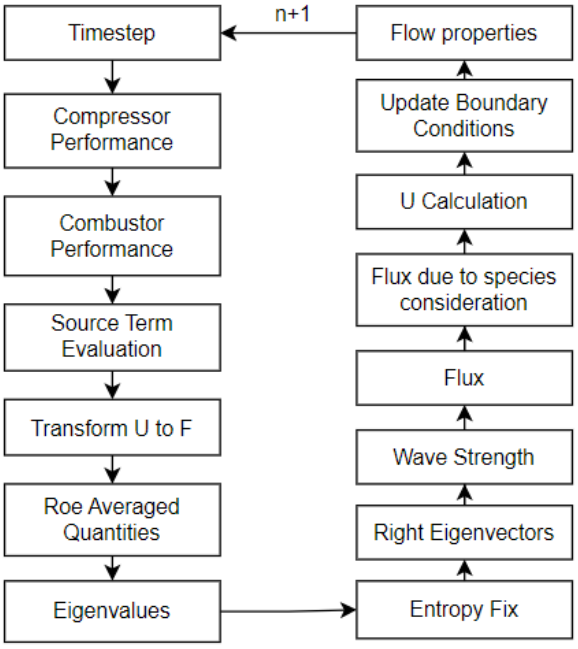


FIGURE 2: COMPUTATIONAL STEPS OF THE MODIFIED ROE SCHEME FOR COMPRESSOR AND COMBUSTOR ONE-DIMENSIONAL SOLVER

The boundary conditions are fixed by specifying the static temperature and pressure at the inlet to the compression and combustion domain. The inlet properties can also be specified to vary

with time. However, by fixing a value, the gas properties at the inlet remains fixed regardless of what is happening inside the domain. This is called a "reflective" boundary which makes the flow transients reflect inside the domain. This could lead to excessive oscillations in flow properties propagating back and forth. Non-reflective boundary condition allows the temporary deviation of properties from those specified. This prevents the reflection of the waves back to the domain.

2.2 Compressor Source Terms

Dynamic compressor performance (F_{comp} and SW) is obtained through the complete compressor characteristics which consist of the forward flow, stall and reverse flow region as shown in Figure 3. The **forward flow** region consists of the typical operating lines of NRT plotted over WRTP against PR and TR. Conventional compressor maps are defined in terms of non-dimensional quantities (WRTP, NRT) which are obtained at the inlet. In steady state conditions, the reference state can be switched from inlet to outlet, knowing the PR and TR, without any consequence. Also, given the ease at which inlet conditions are accurately recorded during testing, there is no pertinent reason to change the reference state. Within the forward flow region, given that the NRT lines tend to choke or become vertical with higher WRTP values, it is more difficult for the compressor solver to accurately find a PR/TR point. Also, a small change in WRTPin would result in big fluctuations of PR and TR being applied to the compressor domain. By switching the reference state to the outlet, the speed lines tend to the x-axis with increasing WRTP. Within this paper, non-dimensional mass flow refers to the compressor's geometrical outlet. The boundary between normal operating conditions and stall is defined by the surge line. They are obtained directly from the manufacturer through extensive testing (depending on the compressor's design phase).

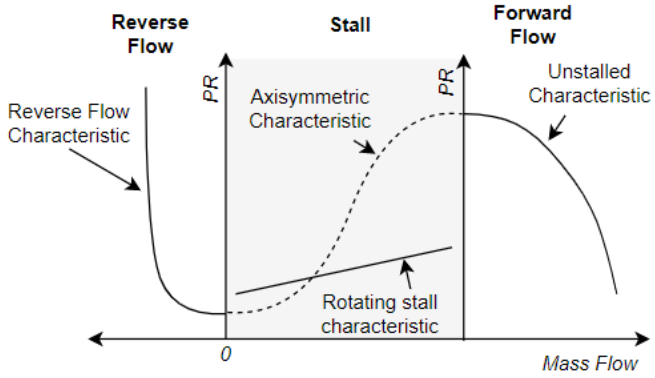


FIGURE 3: COMPLETE COMPRESSOR MAP FOR SIMULATING STALL AND SURGE IN ONE-DIMENSION

The NRT lines within the **reverse flow** region can be obtained experimentally or numerically by fixing a high pressure gradient across the axial compressor which will maintain negative flow throughout. To generate the speed line, various points can be obtained by varying the imposed pressure until flow direction becomes positive. Hence the characteristic can be drawn. The reverse flow lines usually tend to grow vertically exponentially with increasingly negative flow. After a highly negative flow capacity, the geometry imposes a point at which the flow "chokes" regardless of the increasing area at outlet. On the other end, the reverse flow characteristics can be extended until it intersects the point where the non-dimensional mass flow reaches zero. However, based on experimental tests and numerical simulations, recovery happens slightly before WRTP is zero.

The **stall region** is the most difficult to obtain both experimentally and numerically. It is represented by two distinct sets of lines which characterises the operation of the compressor in stall namely the axisymmetric characteristic and the rotating stall characteristic. The rotating stall characteristic is a straight line obtained through the occurrence of mature rotating stall points generated through the slight variation in back pressure at a fixed rotational speed. The line overlaps the forward flow and the reverse flow region which creates some form of hysteresis. Rotating stall is a steady condition whereas the line which represents the axisymmetric characteristic is not. Koff and Greitzer [27] originally proposed the axisymmetric characteristic after inertially correcting experimental surge data. This characteristic is obtained by fitting a cubic curve between the peak of the unstalled characteristic and the lowest point of the reversed flow curve. It is a theoretical characteristic which helps in modelling surge. To model the transition, in time, between the two characteristics, β is introduced. It is controlled by a first-order lag. When entering the stall region from the reverse flow or forward flow characteristics, the flow is first assumed to be symmetric throughout the compressor. An asymmetric structure grows the longer the operating point remains within this region. β is initially set at 0 and grows at a rate defined by the lag factor. A locked in stall case will have β = 1. To reduce excessive numerical instabilities due to fluctuations in the pressure rise or temperature rise obtained from the characteristics, individual first order lag factors are introduced within all regions of the map.

The maps used are pressure ratio, and either temperature ratio or torque maps against non-dimensional mass flow. The temperature ratio maps are used within the unstalled region while torque/inlet pressure maps are used to define the reverse flow and rotating stall characteristics. This change was made to avoid overestimation of temperature rise due to fast transients.

Reverse flow maps and rotating stall characteristics are fed to the solver from the ACRoSS (Axial Compressor Rotating Stall and Surge) tool. It is a three-dimensional through flow code developed at Cranfield University and validated [14,30] for the modelling of rotating stall and surge in both low and high-speed compressors. Using compressor geometry and by running several campaigns in reverse flow and steady rotating stall at various non-dimensional rotational speeds, those maps are generated before being used in the one-dimensional solver.

It is common to use a single set of characteristics to represent a whole axial compressor in a performance model. However, during surge events, gas properties deviate much (spanwise and radially) from the steady conditions which were

used to generate the compressor characteristics. Hence, during flow reversal, the solver switches from using overall to stage-by-stage characteristics. This allows for better representation of axial flow dynamics. To ensure smooth transition between regions, the non-dimensional mass flow, obtained at the geometric outlet, is used to determine which region on the map should be used. If the mass flow changes direction, the switch is made between overall and stage-by-stage characteristics. When only a few stages see positive flow but net flow across the compressor is negative, an approximation of the stage performance of those stages is obtained by estimating stage pressure rise and torque coefficients from the overall rotating stall characteristics. The method used to switch follows Howell and Bonham's simplified method [28].

Based on the calculated non-dimensional mass flow and speed of the compressor, values of pressure rise, and temperature rise can be obtained from the complete compressor maps. The solver can then determine the change in momentum and energy imparted to the flow.

2.3 Plenum Modelling

To test and run stall or surge events on single or multiple compressors, a zero-dimensional plenum was modelled downstream of the compressor. It is advanced in time using the Runge-Kutta 4-step scheme with a set static pressure at outlet boundary condition. The flow velocity inside is assumed to be zero. The modelling is like the one proposed by Greitzer [29] and obtained by Righi [30] who removed the adiabatic assumption and used continuity and energy equations to advance the state of the plenum in time.

2.4 Combustor Source Terms

The simplified one-dimensional combustor model is divided into the cold and hot region. The volume defined approximately matches the total space within both regions. Combustion is modelled as heat transferred within the combustor. Chemical reaction is not modelled due to the extensive computational cost and complexity. Based on the equivalence ratio the amount of combustion products and unburnt fuel can be determined and added to the gas path. Figure 4 gives an overview of the temperature distribution across the one-dimensional combustion model in normal operating conditions.

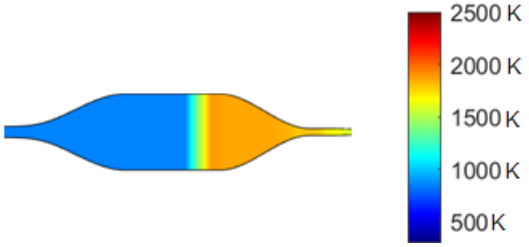


FIGURE 4: TEMPERATURE GRADIENT ACROSS A ONE-DIMENSIONAL COMBUSTOR MODEL USING THE ROE SCHEME

The modelling of the nozzle guide vane has a fixed throat area which limits flow capacity through the gas path. Static pressure is set as the boundary condition which, in normal operating conditions, maintains the throat choked. Changing both the combustor volume and throat area changes surge and stall behaviour.

Fuel is set as an input parameter to the model and based on the inlet conditions to the combustor and its equilibrium performance (through the Numerical Propulsion System Simulation (NPSS)'s chemical equilibrium package), the change in enthalpy is obtained. The heat generated can then be obtained based on inlet mass flow.

A surge or stall event will bring the combustor away from its normal operating conditions. During those events, the heat generated might be overestimated. To account for uncertainties due the one-dimensionality of the model, a combustor efficiency for stall is introduced which can help calibrate the combustor against the actual behaviour of an engine.

3. VALIDATION AGAINST ACROSS

3.1 One compressor in deep surge

A single multi-stage compressor representative of a high-speed compressor was modelled in deep surge. The domain includes a single straight duct followed by the compressor and a smaller duct connected to the plenum. The number of cells is increased along the length of the domain to avoid spurious oscillations. Inputs to the solver define the geometry through the area variation along the length and the number of cells used in the discretization. This is illustrated in Figure 5.

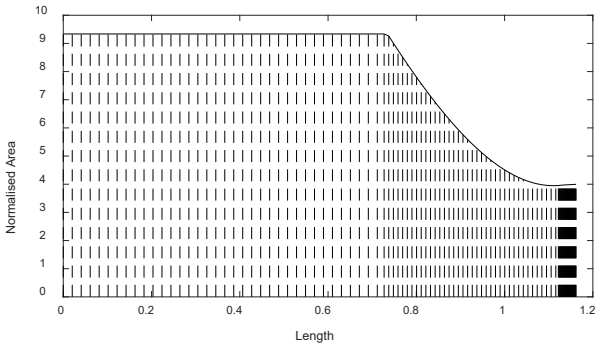


FIGURE 5: ONE-DIMENSIONAL REPRESENTATION OF THE COMPRESSOR DOMAIN

The boundary conditions are specified at the inlet of the domain (static pressure and temperature) and the outlet of the plenum throat where air discharges to a set ambient static pressure. The complete compressor characteristic is inserted as an input. The model is run from an initial guessed flow-field until steady conditions are reached. The throttle at the back of the plenum is then progressively closed until the compressor surges at high speed.

For the same operating and boundary conditions, a two-dimensional surge simulation was performed in ACRoSS. This

was chosen for speed and due to the flow being symmetrical across the circumference of the compressor which improves modelling fidelity of 2D models. The results were compared and are shown in figures 6-9.

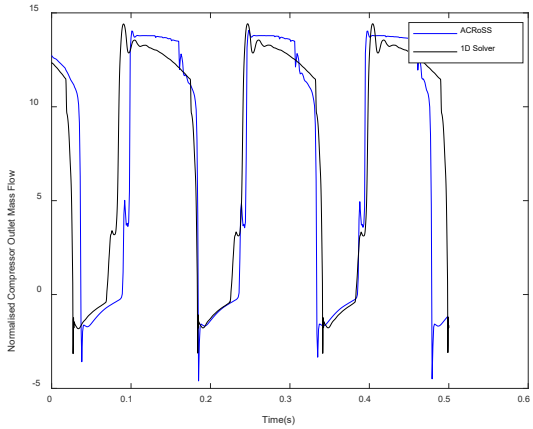


FIGURE 6: MASS FLOW COMPARISON BETWEEN 1D SOLVER AND ACRoSS (2D)

Figure 9 shows the progression of events from the compressor (point 1) being in "quasi" steady state before the surge margin being dropped to initiate surge. The transition between point 1 to point 2 happens very rapidly as the flow within the compressor breaks down from a state of high power and goes into reverse flow (point 2). However due to the presence of rotating blades, the air cannot discharge unrestrained through the front end of the compressor. This is shown by the vertical lines within the reverse flow region of the compressor characteristics. Once the compressor reaches point 2, the pressure ratio across it reduces while the amount of air reversing into the front reduces as well. The movement from point 2 to 3 happens gradually as the pressure at the back reduces. The compressor repressurizes by transitioning from point 3 to 4 and if recovery is possible, the operating point will move from point 4 back to 1.

Given a set of compressor characteristics, the one-dimensional solver replicates results obtained from ACRoSS but at a much lower computational cost (minutes on a regular computer). The surge frequency, amplitude and the blow down are nearly perfectly matched when considering the timescale. The very small difference in the surge frequency might be due to the differences in throttle modelling. A one-dimensional model cannot accurately model the effective area of the nozzle guide vane during various flow conditions as a higher fidelity model would without the use of correction factors. Considering figure 6, the sharp negative mass flow obtained after surge which corresponds to the minimum value follows the same trend in both cases which corresponds to the initial propagation of the pressure wave. Figure 8 shows the sudden increase in total temperature following recovery where hot air is re-ingested.

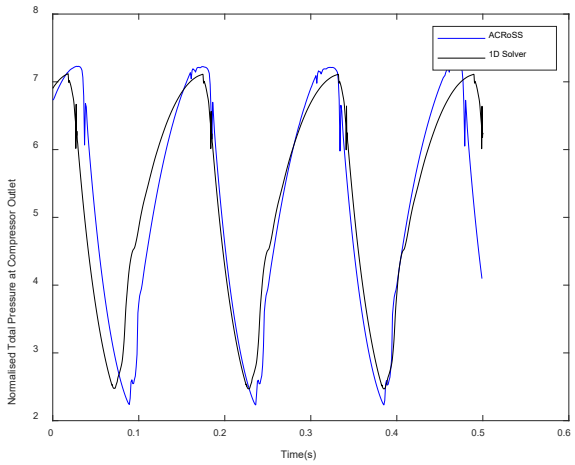


FIGURE 7: TOTAL PRESSURE COMPARISON BETWEEN 1D SOLVER AND ACRoSS (2D)

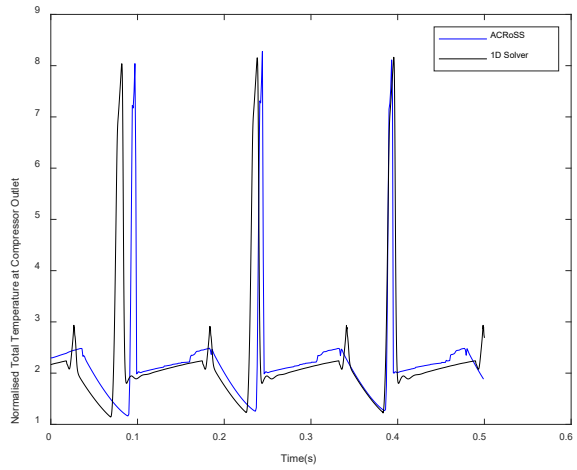


FIGURE 8: TOTAL TEMPERATURE COMPARISON BETWEEN 1D SOLVER AND ACRoSS (2D)

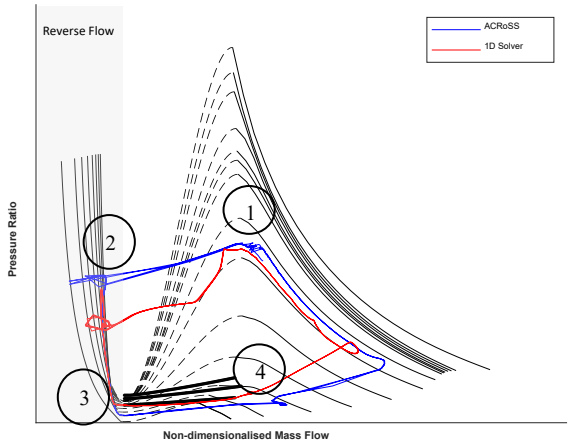


FIGURE 9: COMPARISON OF SURGE CYCLE BETWEEN 1D SOLVER AND ACRoSS ON COMPLETE COMPRESSORS CHARACTERISTIC

3.2 Two compressors in deep surge

The compressor characteristics are generated by points obtained in quasi-steady conditions. This raises the question of whether a one-dimensional simulation code can replicate the performance of multiple compressors in surge using "steady" characteristics. During the on-set of surge, the sudden loss in pressure at the back stages puts more load on the stages which are still in normal operation. This leads to the failure of the front stages which are not able to sustain the sudden rise in load. In case of surge, the compressor will go into reverse flow. With each failing stage, the pressure wave propagating from the back to the front end of the compressor becomes stronger before being discharged through the inlet. Within the case simulated, the HPC is the first one to stall which causes the subsequent stall of the IPC. There is instantaneous flow reversal during the propagation of the surge wave.

Due to the extremely high gas property gradients throughout the compressor, the use of stage-by-stage characteristics was implemented when going into the reverse flow region. This was particularly advantageous when looking at multiple axial compressors in surge.

The verification against ACRoSS was done by considering a typical intermediate and a typical high-power compressor connected in series and discharging to a plenum. The total pressure and temperature are set as boundary conditions at the inlet of the IPC and a static pressure is defined at the throttle exit where complete expansion of the flow is assumed. The throttle volume is specified as 0.25 m^3. Characteristics were obtained by ACRoSS for both compressors for rotating stall and reverse flow at various non-dimensional rotating speeds. The compressors are run at constant speed which is close to design conditions to initiate a deep surge. The results are presented in figures 10 to 13.

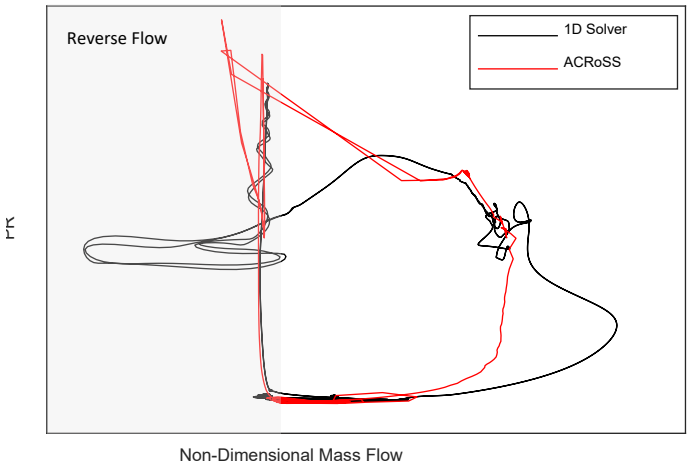


FIGURE 10: IPC MAP COMPARISON BETWEEN 1D SOLVER AND ACRoSS DURING COUPLED IP AND HP COMPRESSORS IN SURGE

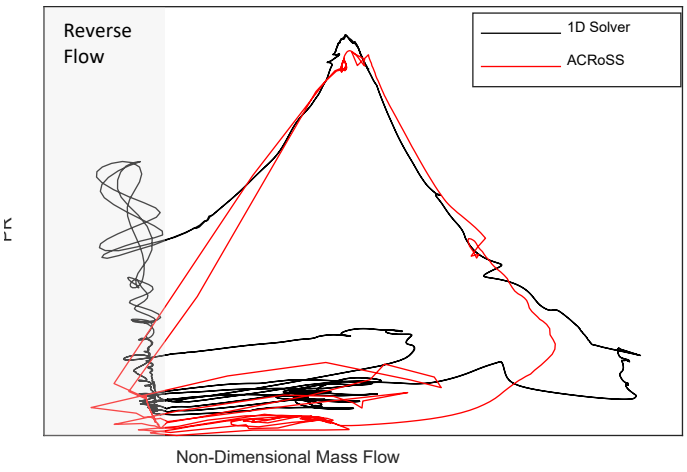


FIGURE 11: HPC MAP COMPARISON BETWEEN 1D SOLVER AND ACRoSS DURING COUPLED IP AND HP COMPRESSORS IN SURGE

Starting from a quasi-steady state point, the HPC was made to surge by slightly closing the throttle at the back of the plenum. Being a deep surge event, the axisymmetric characteristic is mostly used due to the speed at which the operating point transitions from forward flow to reverse flow. When the HPC is in reverse flow, the 1D solver follows more closely the reverse flow characteristic provided compared with ACRoSS which loses pressure faster. Also, the strength of the recovery of the 1D solver is greater. Figures 10 and 11 show this excess in WRTP during recovery within both IP and HP compressors. This overestimation of the non-dimensional mass flow is acceptable due to the limited amount of time that the compressor stays in this region of the map.

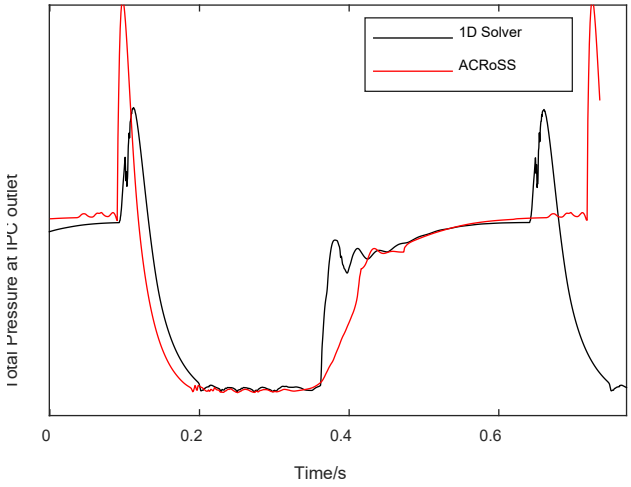


FIGURE 12: COMPARISON OF TOTAL PRESSURE AT IPC OUTLET BETWEEN 1D SOLVER AND ACRoSS DURING COUPLED IP AND HP COMPRESSORS IN SURGE

The pressure wave going from the HPC to the IPC outlet is lower within the 1D solver. However, the blow down rate is matched within 1% for both the IPC and HPC. The surge frequency deviates slightly more. This is due to the small modelling differences in the throttle area between the two solvers. However, in both cases the rate at which both compressors recover follows a similar trend.

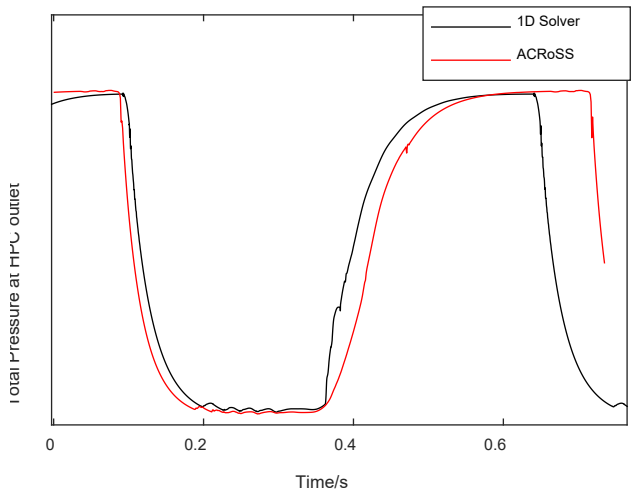


FIGURE 13: COMPARISON OF TOTAL PRESSURE AT HPC OUTLET BETWEEN 1D SOLVER AND ACRoSS DURING COUPLED IP AND HP COMPRESSOR IN SURGE

4. CONCLUSION

A novel one-dimensional code was presented for the simulation of rotating stall and surge. A compressor model representative of an HPC and connected to a plenum was made to go through deep surge at high power. It is compared against the validated through-flow code, ACRoSS. Using rotating stall and reverse flow characteristics the comparison showed close matching against ACRoSS. A second verification case was set up to investigate the applicability of the 1D solver when surge is initiated in a domain of two compressors in series. Two multi-stage compressors representative of an IPC and HPC were connected in series and surge was initiated by closing the throttle. Apart from the strength of the pressure wave during depressurization, close matching was obtained when comparing surge frequency and amplitude. This paper highlights the value of using a low-order model in replicating a highly dynamic event with three-dimensional flow characteristic in only one-dimension. It opens a wide array of opportunities to understand surge and stall behaviour and how factors such as installation, control and compressor design affect behaviour and response. This can be integrated into a whole engine model and numerous iterations are possible within a short time frame. This can open the design space and enhance the scientific community to better understand surge and stall which was previously known as “the most unfortunate occurrence to befall an aero-engine compressor”.

ACKNOWLEDGEMENTS

The authors would like to express their gratitude to Rolls-Royce plc. For funding this research and for permission to publish this research. Special thanks go to Mr Arthur Rowe for their constant support and valuable guidance.

REFERENCES

[1] Day, I. J., 2016, *Stall, Surge and 75 Years of Research*, ASME J. Turbomach., 138(1), p. 011001.

[2] Huppert, M., and Benser, W., 1953, *Some Stall and Surge Phenomena in Axial-Flow Compressors*, J. Aeronaut. Sci., 20(12), pp. 835–845.

[3] Emmons, H., Pearson, C., and Grant, H., 1955, “Compressor Surge and Stall Propagation,” ASME Paper No. 53-A-65.

[4] Moritz, R., 1970, Axial Compressor Stall, von Karman Institute, Belgium, Germany.

[5] Greitzer, E., 1976, “Surge and Rotating Stall in Axial Flow Compressors—Part I: Theoretical Compression System Model,” ASME J. Eng. Gas Turbines Power, 98(2), pp. 190–198.

[6] Greitzer, E., 1976, “Surge and Rotating Stall in Axial Flow Compressors—Part II: Experimental Results and Comparison With Theory,” ASME J. Eng. Gas Turbines Power, 98(2), pp. 199–211.

[7] Gong, Y. 1999, A computational model for rotating stall and inlet distortions in multistage compressors, PhD Thesis, Massachusetts Institute of Technology, Massachusetts, 1999.

[8] M.L. Brand, An Improved Blade Passage Model for Estimating Off-Design Axial Compressor Performance, MSc Thesis, Massachusetts Institute of Technology, Massachusetts, 2013.

[9] J.P. Longley, Calculating stall and surge transients, in: Proceedings of the ASME Turbo Expo 2007: Power for Land, Sea, and Air, Montreal, Canada, May 14–17, 2007, pp.125–136, ASME Paper No: GT2007-27378.

[10] J. Guo, J. Hu, X. Wang, R. Xu, A three-dimensional unsteady through-flow model for rotating stall in axial compressors, in: Proceedings of the ASME Turbo Expo 2020: Turbomachinery Technical Conference and Exposition, ASME, 2020. Virtual, Online. September 21–25, 2020.

[11] H. Zeng, X. Zheng, M. Vahdati, A method of stall and surge prediction in axial compressors based on three-dimensional body-force model, J. Eng. Gas Tur-bines Power 144(3) (2022).

[12] Ju, P., and Ning, F., 2014, “Numerical Investigation of the Prestall Behaviour in a Transonic Axial Fan,” ASME Paper No. GT2014-25502.

[13] Moru, S., Bo, Y., Yueheng, W., Rui, Z. and Zixuan, L. (2022). Analysis on spike-type rotating stall in transonic axial compressor by dynamic mode decomposition. Aerospace Science and Technology, 131(108008), p.108008. doi:10.1016/j.ast.2022.108008.

[14] Righi, M., Pachidis, V., Könözsy, L., Giersch, T. and Schrape, S. (2022). *Experimental validation of a three-*

dimensional through-flow model for high-speed compressor surge. Aerospace Science and Technology, 128(107775), p.107775. doi:10.1016/j.ast.2022.107775.

[15] Roe, P. L., *Approximate Riemann Solvers, Parameter Vectors, and Difference Schemes*, Journal of Computational Physics, Vol. 43, No. 2, 1981, pp. 357–372.

[16] Heiser, W. H., McClure, W. B., and Wood, C. W., *Simulating Heat Addition via Mass Addition in Variable Area Compressible Flows*, AIAA Journal, Vol. 34, No. 5, 1996, pp. 1076–1078.

[17] A. Harten and J. M. Hyman. Self-Adjusting Grid Methods for One–Dimensional Hyperbolic Conservation Laws. J. Comput. Phys., 50:235–269.

1983.

[18] P. L. Roe and J. Pike. Efficient Construction and Utilisation of Approximate Riemann Solutions. In Computing Methods in Applied Science and Engineering. North–Holland, 1984.

[19] P. L. Roe. Sonic Flux Formulae. SIAM J. Sci. Stat. Comput., 13(2):611–630, 1992.

[20] F. Dubois and G. Mehlman. A Non–Parameterized Entropy Fix for Roe's Method. AIAA Journal, 31 (1):199–200, 1993.

[21] Mohanraj, R., Neumeier, Y. and Zinn, B.T. (1999) *Characteristic-based treatment of source terms in Euler equations for Roe Scheme*, AIAA Journal, 37(4), pp. 417–424. Available at: https://doi.org/10.2514/2.749.

[22] Zucrow, M. J., and Hoffman, J. D., *Gas Dynamics*, Wiley, New York, 1976, Vol. 1, Chap. 9, and Vol. 2, Chap. 19.

[23] Ami Harten and James M Hyman. *Self adjusting grid methods for one-dimensional hyperbolic conservation laws*. Journal of Computational Physics, 50(2):235 – 269,1983.

[24] Luca Di Mare. *Modelling of variables gas properties and compositions in turbomachinery flow simulations*. ASME Turbo Expo, GT2008-51085, 2008.

[25] Larrouturou, B. (1991) *How to preserve the mass fractions positivity when computing compressible multi-component flows*, Journal of Computational Physics, 95(1), pp. 59–84. Available at: https://doi.org/10.1016/0021-9991(91)90253-h.

[26] Habbal A., Dervieux A., Guillard H., and Larrouturou B. Inria Report 690 (1987)

[27] Koff, S., and Greitzer, E., 1986, *Axisymmetrically Stalled Flow Performance for Multistage Axial Compressors*, ASME J. Turbomach., 108(2), pp. 216–223.

[28] Howell, A. R., & Bonham, R. P. (2006). Overall and Stage Characteristics of Axial-flow Compressors. *Proceedings of the Institution of Mechanical Engineers*. https://doi.org/10.1243/PIME_PROC_1950_163_026_02

[29] Greitzer, E. M. , 1976, *Surge and Rotating Stall in Axial Flow Compressors, Part I: Theoretical Compression System Model*, ASME J. Eng. Power, 98(2), pp. 190–198.10.1115/1.3446138

[30] Righi, M., Pachidis, V. and Könözsy, L. (2020). *On the prediction of the reverse flow and rotating stall characteristics of high-speed axial compressors using a three-dimensional through-flow code*. Aerospace Science and Technology, 99, p.105578. doi:10.1016/j.ast.2019.105578.

[31] Dodds, J., and Vahdati, M. (May 1, 2015). *Rotating Stall Observations in a High Speed Compressor—Part I: Experimental Study.* ASME. J. Turbomach. May 2015; 137(5): 051002. https://doi.org/10.1115/1.4028557

[32] Moncayo, C. M., de Luna, M. Q., & Ketcheson, D. I. (2022). *A Comparative Study of Iterative Riemann Solvers for the Shallow Water and Euler Equations*. arXiv. https://doi.org/10.48550/arXiv.2209.12235

[33] Leer, B. van (2006), *On the Relation Between the Upwind-Differencing Schemes of Godunov, Engquist–Osher and Roe*, https://doi.org/10.1137/0905001, 5(1), pp. 1–20. Available at: https://doi.org/10.1137/0905001.

[34] Roe, P. L., *Characteristic-Based Schemes for the Euler Equations*, Annual Review of Fluid Mechanics, Vol. 18, 1986, pp. 337–365.



https://dspace.org/

A characteristic-based 1D axial compressor model for stall and surge simulations

Kissoon, Sajal; Righi, Mauro; Pawsey, Lucas; Pachidis, Vassilios; Tunstall, Richard ...

2023-09-09
American Society of Mechanical Engineers (ASME)
https://doi.org/10.1115/GT2023-100709
Kissoon S, Righi M, Pawsey L, et al., (2023) A characteristic-based 1D axial compressor model for stall and surge simulations. In: ASME Turbo Expo 2023: Turbomachinery Technical Conference and Exposition, 26-30 June 2023, Boston, USA

Downloaded from a DSpace repository. https://dspace.org/